Desalination and Water Treatment
www.deswater.com

doi: 10.5004/dwt.2017.20386

67 (2017) 271–283
March

Thermodynamic, equilibrium and kinetic studies of adsorption of Rhodamine B onto activated bamboo carbon

Buddhika Gayani[a], A.D.L. Chandani Perera[b], Nilwala Kottegoda[a,c,d,*]

[a]*Department of Chemistry, University of Sri Jayewardenepura, Gangodawila, Nugegoda, Sri Lanka, Tel. 0094773830313; emails: nilwala@sjp.ac.lk, nilwalak@slintec.lk (N. Kottegoda), Tel. 0094716455954; email: gdbgayani1@gmail.com (B. Gayani)*
[b]*Department of Chemistry, University of Peradeniya, Peradeniya, Sri Lanka, Tel. 0094773594127; email: chandanip@pdn.ac.lk*
[c]*Sri Lanka Institute of Nanotechnology, Center for Excellence in Nanotechnology, Pitipana, Homagama, Sri Lanka*
[d]*Advanced Material Research Center, Faculty of Applied Sciences, University of Sri Jayewardenepura, Gangodawila, Nugegoda, Sri Lanka*

Received 4 May 2016; Accepted 25 November 2016

ABSTRACT

Activated bamboo carbon (ABC) was chemically synthesized using phosphoric activation method, and the resulting material was used to remove Rhodamine B from aqueous solutions. The surface characteristics of the ABC were studied, and the conditions for the maximum removal of dye were established. The capacity of Rhodamine B removal from ABC was 100% for a system with 0.02 g of ABC and initial Rhodamine B concentration of 50 mg L^{-1} at 300 K. The best-fit adsorption isotherm was Langmuir model with maximum adsorption capacity of 111.11 mg g^{-1} at 300 K. The L4-type adsorption suggests that at low Rhodamine B concentrations, adsorption occurs in a flat orientation and becomes end-on orientation at higher concentrations. Thermodynamic data reveal that the adsorption process is endothermic with increasing entropy and moderately large negative free energy values indicate the feasibility of the adsorption process. Pseudo-second-order kinetic model fitted well to both adsorption and desorption processes suggesting the rate-limiting step involves chemical interactions. Furthermore, intraparticle diffusion model indicates the simultaneous occurrence of three diffusion steps caused by external mass transfer to the bulk solution, intraparticle diffusion and desorption of the adsorbed dye molecules.

Keywords: Activated bamboo carbon; Adsorption; Rhodamine B; Kinetic models; Isotherms; Nano-porous; Thermodynamic study

1. Introduction

Maintaining water quality standards is becoming a global concern due to the depletion of limited freshwater resources as a result of anthropogenic activities with increasing global population. Therefore, there is an increased need for development of cost-effective, environmental-friendly and efficient water treatment methods [1–6]. Activated carbon is an excellent adsorbent widely used in advanced water treatment applications due to the availability of low-cost raw materials in production processes, efficient multipollutant removal and regeneration abilities. There is a wide range of low-cost raw materials: agricultural wastes [7], carbonaceous materials such as sawdust [8], rice husk [9], peanut shell [10] and coconut nut shell [11] suitable for the synthesis of activated carbon.

Rhodamine B (RhB) is used as a dye in many industries such as textile, bamboo, toys, handicraft, leather, paper and biological laboratories. Wastewater discarded from such industries contains a considerable amount of RhB, which can badly affect the aquatic environment lowering the transparency of water hindering the photosynthesis of aquatic plants. When RhB contacts with the skin, it causes skin irritation, and longer time exposure can cause cancers. Although various

* Corresponding author.

methods including photocatalytic degradation are used for purification of dye containing effluents [12,13], a simple low-cost adsorption process would be more effective. One such method is adsorption onto activated carbons derived from low-cost raw materials.

Significant research attempts have been made to develop methods for removal of RhB using various types of cellulose based materials. Chieng et al. [14] reported the use of peat to remove RhB from aqueous solutions obtaining a maximum adsorption capacity (q_{max}) of 162.87 mg g^{-1} at 298 K. In another study, Hossain and Alam [15] used black tea leaves for the purpose of RhB removal and obtained a lower adsorption capacity of q_{max} of 53.2 mg g^{-1} at pH 2.0. Activated carbons derived from natural matter were reported to be more effective for the adsorption of RhB than natural matter themselves, e.g. *Phoenix sylvestris* leaves had been activated using sulphuric acid activation method by Arivoli and Henkuzhali [16] and obtained q_{max} of 51.55 mg g^{-1} whereas sulphuric acid activated *Thespesia populnea* bark [17] yielded q_{max} of 60.84 mg g^{-1} for removal of RhB. Li et al. [18] used activated pyrolytic tire char for the adsorption of RhB dye and found that the adsorption obeys Langmuir isotherm with a higher adsorption capacity of q_{max} of 307.2 mg g^{-1} at 45°C. In another study, palm shell, which has high lignin content of 54%, has been activated using CO_2 followed by NaOH activation [19] achieving a maximum RhB removal of 95% at an initial RhB concentration of 62.6 μmol dm^{-3} at pH 3 and temperature of 50°C. These studies clearly emphasize the possibilities of enhancing the percentage removal of RhB using activated carbon derived from naturally available carbonaceous materials. Out of the many such materials, bamboo is a potential candidate for the preparation of effective activated carbon. Bamboo can be used as a cheap raw material in activated carbon industry as it is readily available in a wide range of geographical variations and the possibility to convert bamboo wastes to a low-cost value-added product. Bamboo activated carbon has been already used for heavy metal removal [20], methylene blue removal [21,22] and antimicrobial applications [23].

We have previously reported the successful use of activated carbon derived from coconut coir for desalination, hardness removal and deflouridation applications [24–26]. This research is a further extension to explore low-cost sources for production of activated carbon for various water purification applications. Here, we report, the use of activated bamboo carbon (ABC) originated from *Bambusa vulgaris* precursors for the efficient removal of RhB from aqueous solutions. Kinetic and thermodynamic aspects of the adsorption process has also been investigated. Phosphoric acid activated bamboo charcoal has been selected considering its rich surface chemistry and affinity towards many water pollutants while RhB has been used as the model molecule since it is one of the major sources of water pollutant in textile effluent. Therefore, this work attempts to initiate a timely study to look for locally viable economical solutions to address the issue.

2. Experimental details

2.1. Reagents

All chemicals used throughout the experiments were of analytical grade and procured from Techno Pharmchem Haryana Chemicals, Research-Lab Fine Chem Industries and Lobachemie Chemicals from India. Whatman filter paper of size 40 μm was used for filtering purpose. Distilled water and distilled ethanol were used as solvents in the experimental work. RhB (molar mass of 479.02 g mol^{-1}) was purchased from Research-Lab Fine Chem. Commercial activated carbon (CAC) made of coconut shells with an iodine number of 1,100 mg g^{-1} was obtained from Haycarb PLC, Sri Lanka.

2.2. Synthesis of activated bamboo carbon

Phosphoric acid activation method was used to activate bamboo sawdust (collected from *Bambusa vulgaris*) according to the literature [27]. Dried bamboo sawdust (5.00 g) was soaked in 85% (w/w) phosphoric acid (weight ratio of 1:1), well agitated and allowed to digest for 48 h at room temperature. The residue was heated to 600°C at a heating rate of 10°C min^{-1} in a Muffle furnace. A nitrogen flow at a rate of 40 mL min^{-1} was purged during the heating to minimize the reaction with atmospheric oxygen. After the pyrolyzation, the samples were cooled down to room temperature under nitrogen flow. Then, activated samples were washed with distilled water until pH value of the medium reaches 6 and dried at 105°C for 12 h. The carbon yield was calculated using:

$$\text{Yield } \% = \frac{w_f}{w_0} \times 100 \quad (1)$$

where w_f is the final weight of the dried ABC sample, and w_0 is the initial weight of bamboo precursor.

2.3. Characterization

2.3.1. Boehm titration

The surface acidic/basic groups were analyzed using Boehm titration as explained by Boehm [28]. ABC (0.12 g) was placed in five 250.00-mL stoppered flasks and standardized solutions (20.00 mL of 0.05 mol dm^{-3}) of NaOH, Na_2CO_3, $NaHCO_3$, HCl and distilled water were added to each flask, separately. The content was degassed with nitrogen and shaken for 48 h. The basified activated carbon was filtered and titrated with 0.05 mol dm^{-3} HCl solution. The acidified activated carbon was filtered and titrated with 0.05 mol dm^{-3} NaOH solution. The reacted amounts of acidic and basic functional groups were calculated. All readings were triplicated and averaged. The same procedure was performed with CAC (0.12 g) to identify surface acidic/basic groups.

2.3.2. Iodine number determination

For analysis of micro-/nano-porous surface area, the iodine number was determined using 0.5 g of ABC according to American Society for Testing and Materials standards (D 4607-94) [29]. HCl acid (10 mL of 5 wt%) was added to ABC and swirled gently until ABC was completely wetted. The content was boiled for 30 s to remove sulphur, which may interfere with the test results, and then, left to cool to room temperature. A volume of 100 mL of 0.1 N iodine solution was added to ABC and shaken for 30 s. The mixture was

quickly filtered, and 50.00 mL of the filtrate was titrated with a standardized 0.1 N $Na_2S_2O_3$ solution until colourless using 2 mL of starch as the indicator.

$$A = N_2 \times 12693 \tag{2}$$

$$B = N_1 \times 126.93 \tag{3}$$

$$DF = \frac{\lfloor I + H \rfloor}{F} \tag{4}$$

$$\text{Iodine number} = \frac{\left[A - \lfloor DF \times B \times S \rfloor \right]}{M} \tag{5}$$

where N_1 is the normality of $Na_2S_2O_3$ solution; N_2 is the normality of iodine solution; I is the volume of iodine solution; H is the volume of 5% HCl solution; F is the volume of filtrate; S is the volume of $Na_2S_2O_3$ solution; and M is the mass of the carbon.

2.3.3. FTIR analysis

Fourier transform infrared (FTIR) spectra were used for identification of the surface functional groups. FTIR spectra were recorded between 4,000 and 600 cm^{-1} with a resolution of 600 by averaging 32 scans using Nicolet IS 10 instrument. Attenuated total reflection mode was used for data collection.

2.3.4. Powder X-ray diffraction

Powder X-ray diffraction (PXRD) patterns were analyzed to determine the crystallographic characteristics of ABC and CAC. PXRD analysis was conducted using Bruker D8 focus X-ray powder diffractometer using Cu Kα radiation (λ = 1.540 Å) over 2θ angle of 2°–70° with a step size of 0.02°.

2.3.5. Transmission electron microscopy

Transmission electron microscopy (TEM) analysis was carried out using JEOL JEM 2100 microscope operating at 200 kV. The samples were dispersed in methanol and loaded on Lacey carbon-coated copper grids (300 mesh). The sample containing grids were dried for 24 h at room temperature prior to analysis.

2.3.6. Energy-dispersive X-ray analysis

Elemental analysis was carried out by using energy-dispersive X-ray (EDX) mode attached HITACHI SU 6600 SEM with an acceleration voltage of 15.0 kV. Samples were coated with a thin layer of gold prior to analysis, and observations were conducted in the secondary electron mode.

2.3.7. Point of zero charge of ABC

Point of zero charge (pH_{pzc}) of ABC was determined by mass titration method [30]. Different amounts of activated carbon were put into 0.1 mol dm^{-3} NaCl solutions (10 mL), degassed and stoppered. The contents were shaken in Clifton shaker at 200 rpm at 300 K. After 24 h, the equilibrium pH values were measured.

2.4. Adsorption studies

2.4.1. Effect of contact time

A solution of RhB (25.00 mL) with initial concentration of 50 mg L^{-1} was added into a series of flasks containing ABC (0.02 g). The contents were shaken in a water bath at a constant speed of 200 rpm at constant temperature of 300 K. Flasks were taken out at 15 min intervals for a time period of 120 min, and a constant volume (12.50 mL) from each solution was centrifuged for 15 min. The content was left for 1 h to be settled. Then, the supernatant was pipetted out, and the extent of RhB adsorbed was determined using UV-visible spectrophotometer (UV-2602 Labmed) at λ_{max} of 554.0 nm. The experiment was triplicated, and the contact time to reach the equilibrium was determined. The percentage of removal was calculated using:

$$\text{Removal \%} = \frac{C_0 - C_e}{C_0} \times 100 \tag{6}$$

where C_0 and C_e (mg L^{-1}) are the initial and equilibrium concentrations of RhB, respectively.

2.4.2. Effect of pH

A series of solutions of 80 mg L^{-1} RhB of varying pH (pH 3–12) were prepared by maintaining the alkalinity using dilute NaOH and acidity using dilute HCl.

Then, prepared RhB solutions (25.00 mL) were added into flasks containing 0.02 g of ABC, and the contents were shaken in a water bath at a constant speed of 200 rpm at a constant temperature of 300 K until the equilibrium was reached. After that, a constant volume (12.50 mL) from each solutions was centrifuged and left for 1 h, and the extent of RhB adsorbed was determined using UV-visible spectrophotometer at λ_{max} of 554.0 nm. The percentage of RhB removal was calculated at different pH. All measurements were triplicated.

2.4.3. Effect of initial concentration

A concentration series of RhB with initial concentrations from 0 to 1,000 mg L^{-1} was prepared by adjusting the pH to 4. The prepared solutions (25.00 mL) were added into flasks containing 0.02 g of ABC. Then, the same procedure mentioned in section 2.4.2 was followed to determine the extent of RhB adsorbed to ABC. The uptake of RhB at equilibrium q_e (mg g^{-1}) was calculated:

$$q_e = \frac{\left(C_0 - C_e\right)}{C_0} \times 100 \tag{7}$$

where C_0 and C_e (mg L^{-1}) are the initial and equilibrium concentration of RhB, respectively.

2.4.4. Adsorption isotherm models

A series of RhB solutions with initial concentrations ranging from 0 to 200 mg L^{-1} were prepared by adjusting the pH to 4. The solutions (25.00 mL) were added into flasks containing 0.02 g of ABC. Then, the extent of RhB adsorbed to ABC was determined using the same procedure mentioned in section 2.4.2.

This data was used to construct the isotherms for adsorption process (Table 1). All four experiments mentioned in sections 2.4.1–2.4.4 were carried out at four different temperatures of 300, 310, 320 and 330 K. The data were fitted to Langmuir, Temkin, Freundlich, *Dubinin–Radushkevich* (D–R) and Sips models, and relevant physical parameters were calculated in order to explain the interactions between the adsorbent and the adsorbate.

2.4.5. Thermodynamic studies

The thermodynamic parameters such as standard Gibbs energy ($\Delta G°$, kJ mol^{-1}), enthalpy ($\Delta H°$, kJ mol^{-1}) and entropy ($\Delta S°$, J K^{-1} mol^{-1}) changes were determined using RhB solutions with initial concentration of 80 mg L^{-1} using the following equations:

$$K_0 = \frac{C_{solid}}{C_{liquid}} \tag{8}$$

$$\Delta G° = -RT\ln K_0 \tag{9}$$

$$\ln K_0 = \frac{\Delta S°}{R} - \frac{\Delta H°}{RT} \tag{10}$$

where K_0 is the distribution coefficient; C_{solid} is the solid phase concentration (mg L^{-1}) at equilibrium; C_{liquid} is the liquid phase concentration (mg L^{-1}); $\Delta G°$ is the Gibbs energy; T is the absolute temperature; R is the gas constant; $\Delta S°$ is the entropy change and $\Delta H°$ is the enthalpy change of the system.

2.5. Kinetics studies – adsorption and desorption

2.5.1. Adsorption kinetics

ABC (0.10 g) was shaken with 125.00 mL of RhB (125 mg L^{-1}) at the temperature of 300 K and pH of 4.0. A known volume (4.00 mL) was pipetted out from the solution at 5 min intervals for 60 min until the equilibrium was reached. The extent of RhB adsorbed was determined using UV-visible spectrophotometer at λ_{max} of 554.0 nm. The readings were triplicated for each withdrawal, and adsorption of RhB at time t (q_t) was calculated using Eq. (11):

$$q_t = \frac{(C_0 - C_t)V}{W} \tag{11}$$

where C_0 and C_t (mg L^{-1}) are the desorbed or adsorbed concentrations of RhB initially and at time t respectively; V (L) is the volume of RhB solution; and W (g) is the mass of ABC.

2.5.2. Desorption kinetics

ABC (0.12 g) was shaken with 125.00 mL of RhB (125 mg L^{-1}) at the temperature of 300 K and pH of 4.0 until the equilibrium was reached. Then, the content was filtered and washed with distilled water to remove excess RhB, which was not adsorbed. The residue was air dried in dark to avoid photo degradation for 24 h.

Distilled 95 wt% ethanol (125.00 mL) was added into 0.1 g of the above dried sample and shaken at a constant speed of 200 rpm at constant temperature of 300 K. A known volume (4.00 mL) was pipetted out from the solution at 5 min intervals for 45 min until the equilibrium was reached. The extent of desorbed RhB was determined using UV-visible spectrophotometer at λ_{max} of 545.0 nm. The readings were triplicated for each withdrawal and release of RhB at time t (q_t) was calculated using Eq. (11).

3. Results and discussion

3.1. Characterization of ABC

Formation of high surface area of ABC was suggested by the iodine value of ABC (~1,100 mg g^{-1}) which is similar to that of CAC and the nano-ranged pore sizes observed by the transmission electron microscopic analysis.

It was hypothesized that phosphoric acid activation leads to formation of different sized pores containing both acidic and basic functional groups. The nature of the available functional groups was identified referring to the Boehm titration and FTIR characterization results (Table 2). Boehm titration confirmed the presence of carboxylate (0.75 meq g^{-1}), lactones (0.58 meq g^{-1}), phenols (0.42 meq g^{-1}) and basic groups (0.63 meq g^{-1}) in ABC [31]. The amounts of lactone, carboxylic acid and basic functional groups in ABC were higher than those in coconut shell activated carbon.

FTIR characterization further provides evidences for the presence of functional groups (Fig. 1). The FTIR spectrum for ABC shows broad peaks above 3,400 cm^{-1} and at 2,981–2,941 cm^{-1} which are assigned to phenolic O–H stretching and carboxylic O–H and adsorbed water stretching, respectively. FTIR peaks around 1,700 cm^{-1} appear due to stretching of various C=O species such as ketones, aldehydes and carboxylic acids while FTIR peaks around 1,320–1,000 cm^{-1} arise due to C–O stretching of alcohols, carboxylic acids, esters and ethers.

Table 2
Amount of surface functional groups on ABC

Functional groups	Concentration ± 0.01 (meq g^{-1})		FTIR peak position (cm^{-1}) [29,32]
	ABC	CAC	
Carboxylates	0.75	0.60	1,120–1,200
			1,665–1,760
			2,500–3,300
Lactones	0.58	0.05	1,160–1,370
Phenols	0.42	0.75	1,000–1,220
			2,500–3,620
Basic	0.63	0.45	950–1,200

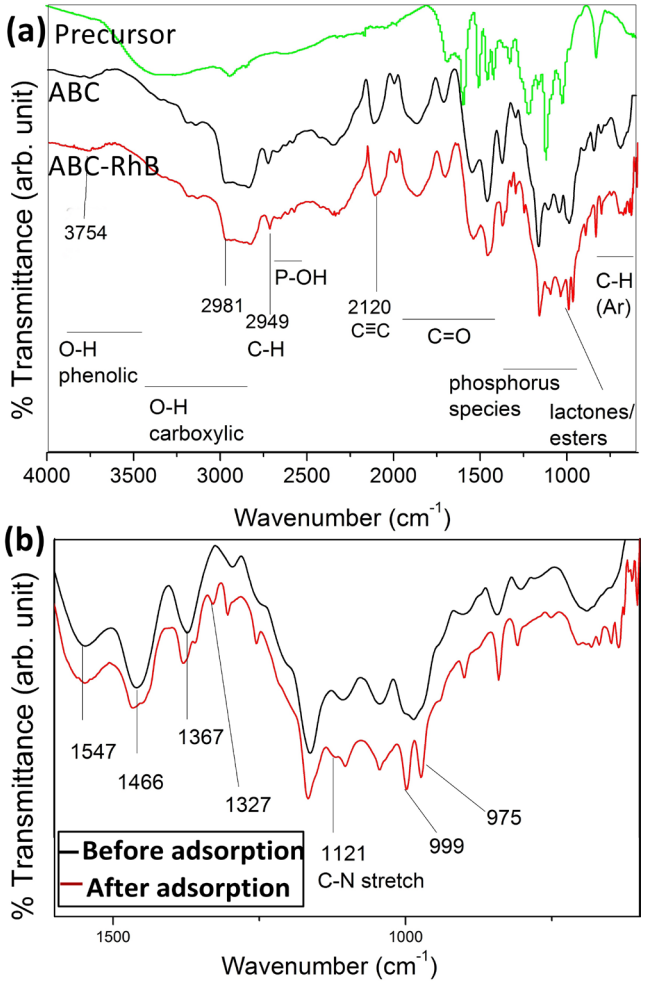

Fig. 1. FTIR spectra for: (a) bamboo precursor, ABC before adsorption of RhB, and ABC after adsorption of RhB and (b) ABC before and after adsorption of RhB (expanded spectrum <1,700 cm^{-1} emphasizing the peak shifts.

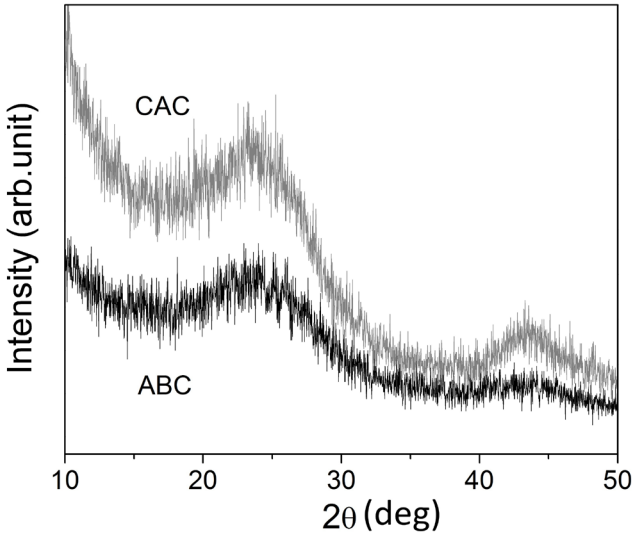

Fig. 2. PXRD patterns of CAC and ABC.

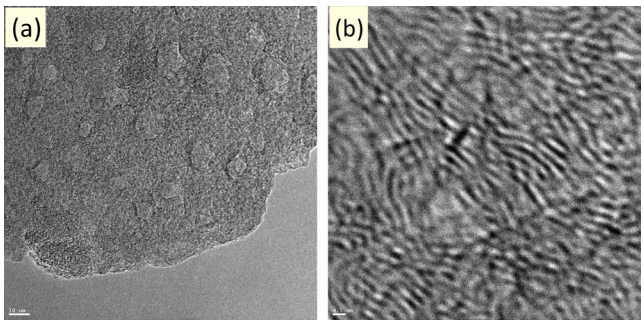

Fig. 3. TEM images of ABC (a) amorphous structure at high magnification (10 nm scale) and (b) disordered layered structure (scale bar represents 1 nm).

This confirms the presence of phenol, carboxylic acids and lactone functional groups on ABC surface. The peak appearing at 2,260–2,100 cm^{-1} is due to C≡C stretching indicating the presence of alkyne functional group on ABC surface. Below 900 cm^{-1}, FTIR peaks arise due to C–H bending modes of alkenes and aromatics. Peaks appearing at 2,800–2,500 cm^{-1}, 1,300–900 cm^{-1} and 754–634 cm^{-1} could be assigned to various phosphate bonding modes such as P–O–H, P=O, P–O–C aromatic linkage, P=OOH and P–C, which indicate the phosphoric esters and ethers arising as a result of phosphoric acid activation process [32]. After adsorption of RhB onto the surface of ABC, new peaks appear at 1,327 cm^{-1} (C–O stretching), 1,121 (N–H stretching) and below 1,000 cm^{-1} (C–H bending of C=C) indicating the adsorption of RhB. Also, the shifting of peaks at 1,466, 1,367 and 1,293 cm^{-1}, and peaks below 1,000 cm^{-1} to higher wave numbers indicate the modifications of carbonyl groups and alkene groups, respectively. Thus, electron density change has occurred when RhB adsorb to the surface of ABC exhibiting chemisorption.

PXRD analysis was used to determine the crystallographic features of ABC. In ABC, the diffraction peak centered at 2θ of 24.02° (Fig. 2) is attributed to 002 plane while in CAC, the diffraction peaks centered at 2θ of 23.60° and 43.34° are attributed to 002 and 101 planes of the graphitic carbon. Generally, in activated carbon, graphene layers are stacked in parallel as translated and rotated layers without having a three-dimensional ordering. These deviations result in number of small domains of parallel stacked layers, which causes for line broadening of 002. The 101 orientation is arisen due to the zigzag formation of edges, which is caused by the one atomic layer edge pits [28]. The value of interlayer distances (d_{002}) between two planes were found to be 0.370 nm for ABC and 0.380 nm for CAC, which were closer to the standard interlayer spacing of pure graphitic carbon. The low intensity and broad peaks suggest an amorphous nature for both ABC and CAC.

Imaging techniques were used to study the surface characteristic features and nature of pores present. TEM images show a highly porous structure formed with graphene layers. The high surface area of ABC is due to the uneven surface morphology as shown in Fig. 3(a) and the availability of irregular shaped nano-pores with a diameter of below 20 nm. The graphitic layers, which are stacked in parallel but translated and rotated in an irregular way, are clearly observed in

TEM. The interlayer spaces are found to be 0.370 nm, corroborating the PXRD evidences. The thickness of the graphene layers are approximately 0.35 nm as depicted in the Fig. 3(b). Therefore, ABC consists of complex pore structure with nano-pores derived from fractures between graphitic layers that can be effectively used as a multipurpose adsorbent. As a result of micro-/nano-porosity, a higher iodine number was obtained.

Quantitative elemental analysis was carried out using EDX analysis. ABC consists of *P* (3.99%), which is absent in bamboo precursor; it is originated due to phosphorous activation (Table 3). Pyrolysis has also caused for higher carbon percentage (76.27%) than bamboo precursor. After adsorption of RhB, high nitrogen percentage (62.75%) was observed due to the nitrogen molecules available in RhB. The lowering of the percentages of other elements (C, O, P, K etc.) is due to the ABC surface covering by RhB molecules. On the other hand, CAC consists of the highest carbon percentage (92.38%) and the least oxygen percentage (4.69%) indicating the low availability of surface oxygenated functional groups.

The pH_{pzc} value of ABC was 2.14 (Fig. 4), which is lower than those reported for the same activation method [30]. The high acidic pH_{pzc} could be due to the presence of acidic functional groups such as carboxylic on the ABC's surface. This acidic value could also be due to that the phosphoric acid, which has not been removed thoroughly by washing [33].

ABC prepared in this study has a graphitic layered structure, highly porous with different size pores ranging from submicro- to nano-scale thus, leading to a high surface area, consists of both basic and acidic functional groups as confirmed by Boehm titration and active functional groups such as alcohols, phenols, carboxylic acids, alkynes, alkenes, esters, ethers, phosphate ethers and phosphate esters as confirmed by the FTIR technique. The adsorption of RhB by ABC was studied in order to understand its effectiveness as an adsorbent.

3.2. Adsorption studies

3.2.1. Effect of contact time

The effect of contact time for adsorption of RhB onto ABC was determined by shaking ABC in RhB solution for different time intervals up to 120 min followed by 1 h settling time to ensure that full equilibrium has reached, as the system would undergo slow processes such as various mass transfer or diffusion steps [20].

Until 60 min, the adsorption of RhB onto ABC increased rapidly (Fig. 5(a)) due to the availability of large number of vacant sites on the external surface of the adsorbent. Initially, RhB molecule, which has a length of 1.8 nm and a width of 0.7 nm [20], easily penetrate through the meso-/nano-pores present in ABC. Thereafter, adsorption slows down, due to the repulsive forces exerted by the already adsorbed RhB molecules. After 90 min, the percentage of RhB removal reaches a constant value by attaining 100% removal efficiency. Thus, the optimum contact time for all experiments was taken as 105 min including 90 min shaking time and 15 min centrifuging time and then left for 1 h to be settled.

3.2.2. Effect of PH

The rate of adsorption of RhB on activated bamboo surface is pH dependent. The pH value of the medium determines the surface charge, dye binding sites on the

Table 1
Linear forms of adsorption isotherms

Isotherm type	Linear form	Plot
Langmuir	$\frac{C_e}{q_e}=\frac{1}{K_L q_{max}}+\frac{C_e}{q_{max}}$	$\frac{C_e}{q_e}$ vs C_e
Freundlich	$\ln q_e=\frac{1}{n}\ln C_e+\ln K_F$	$\ln q_e$ vs. $\ln C_e$
Temkin	$q_e=B\ln K_T+B\ln C_e$ $B=\frac{RT}{b_T}$	q_e vs. $\ln C_e$
D–R	$\ln q_e=\ln q_{max}-\beta\epsilon^2$ $\varepsilon=RT\ln\left[1+\frac{1}{C_e}\right]$ $E=\frac{1}{\sqrt{2\beta}}$	$\ln q_e$ vs. ϵ^2
Sips	$\ln\frac{q_e}{q_{max}-q_e}=\frac{1}{n}\ln C_e+\ln K_S$	$\ln\left(\frac{q_e}{q_{max}-q_e}\right)$ vs. $\ln C_e$

Note: q_e is the adsorption capacity at equilibrium (mg g^{-1}); q_{max} is the maximum adsorption capacity (mg g^{-1}); C_e is equilibrium concentration of the adsorbate (mg L^{-1}); K_L is Langmuir constant (L mg^{-1}); K_F is Freundlich constant (mg g^{-1}); $1/n$ is heterogeneity factor; K_T is the equilibrium binding constant for the maximum binding energy (L mg^{-1}); b_T is Temkin isotherm constant; R is universal gas constant (J mol^{-1} K^{-1}); T is absolute temperature (K); B is constant related to heat of sorption (J mol^{-1}); β gives mean free energy; E is the sorption per molecule of sorbate; and K_s is the Sips constant (L mg^{-1}).

Table 3
EDX analysis data

Sample	Atomic percentage (%)								
	C	O	N	P	Si	K	Cl	Mg	Ca
Bamboo precursor	58.72	39.62	0.00	0.00	0.19	0.77	0.63	0.07	0.13
ABC	76.27	18.46	0.00	3.99	0.99	0.08	0.01	0.05	0.00
RhB adsorbed ABC	29.34	7.15	62.75	0.30	0.43	0.00	0.00	0.00	0.03
CAC	92.38	4.69	0.00	1.14	0.52	0.91	0.00	0.04	0.19

surface and degree of ionization of the dye molecule [14]. RhB is an aromatic amino acid that has positive charge on one of the nitrogens in aqueous solutions. In a polar solvent, the RhB molecules exist in cationic form (RhB^+) or zwitterion form ($RhB^{\pm}$). Ion pair containing RhB^+ form dimers at near neutral pH values via electrostatic interactions between carboxyl and xanthane groups of the monomers [16].

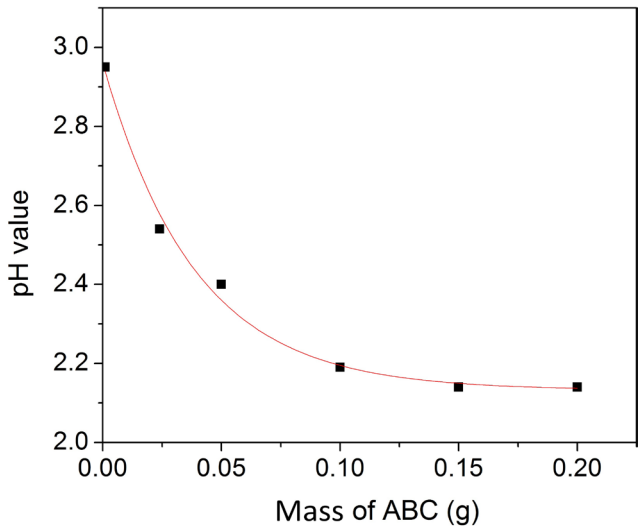

Fig. 4. Determination of pH_{pzc} value.

The adsorption of RhB onto ABC is high up to pH 6 showing higher removal capacity (>80%). Since pH_{pzc} is 2.14, the ABC surface is negative for the measured range of pH 3–12 (Fig. 5(b)). Therefore, the positive charge on amine of RhB molecule can be attracted onto ABC surface via electrostatic interactions. With increasing pH, RhB molecules deprotonize, and zwitterions ($RhB^{\pm}$) are formed. Thus, both acidic and basic surface functional groups on ABC can attract more RhB molecules allowing them to be adsorbed on the ABC surface. However, lower adsorption was observed at pH 7, since the zwitterions formed ($RhB^{\pm}$) undergo dimerization at this pH value. As the aggregation occurs, RhB dimer is unable to enter the smaller pores, hinders penetration and thus decreases dye adsorption on pore walls [14]. With increasing pH above 8, deprotonization of RhB molecules could cause formation of negative charge on the dye molecule (RhB–) reducing the ability of negative ABC to attract on the surface. The observed trend of the percentage removal of RhB on pH is in good agreement with the observed pH_{pzc} value of 2.14.

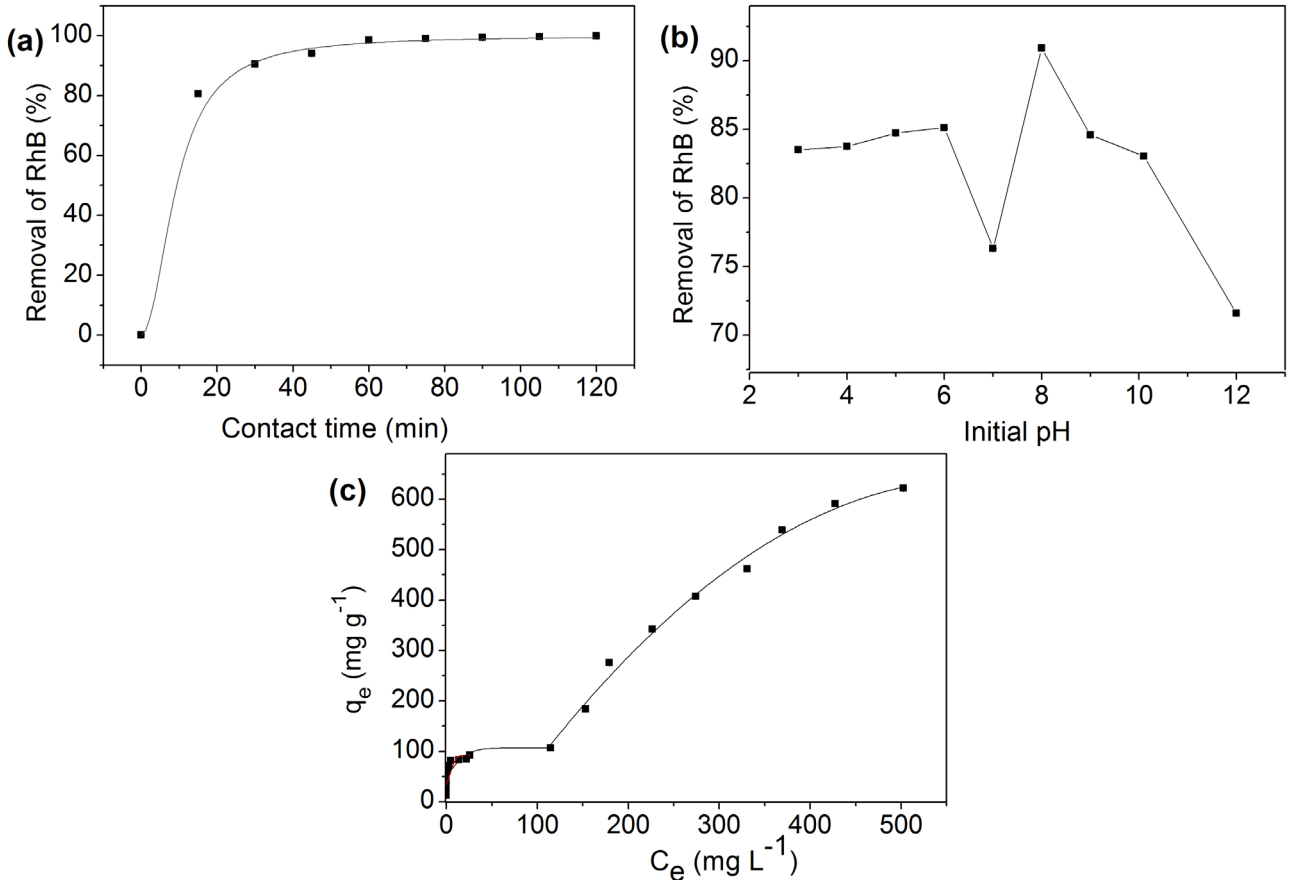

Fig. 5. Effect of adsorption conditions for ABC amount of 0.02 g mL^{-1} at 300 K (a) contact time in [RhB] = 50.0 mg L^{-1}, (b) pH value in [RhB] = 80.0 mg L^{-1} and (c) initial concentration.

3.2.3. Effect of initial concentration of RhB

The adsorption capacity of RhB on ABC was determined at different initial concentrations from 10 to 1,000 mg L^{-1} (Fig. 5(c)). Adsorption of RhB onto ABC follows L4 type, which is similar to adsorption process of phenol on graphite [34]. Although L4 type is less common than other L types, similar type of findings has also been reported by other researchers [35–37]. This process occurs when the orientation is initially flat at low concentrations, and at higher concentrations, the molecules attach at end-on in vertical orientation. According to Giles et al. [34], in order to form L-type system, the adsorbate molecule should structurally be adsorbed flat. In order to adsorbate to be end-on orientation, solvent competition should be minimized, and this can be fulfilled by highly polar surface and adsorbate molecules in a non-polar solvent or mono-functional ionic adsorbate molecules attached to the surface with very strong intermolecular interactions (Fig. 6).

In the RhB–ABC system, the optimum stability is gained at its flat orientation since RhB can be stabilized by hydrophobic interactions formed between aromatic ring of RhB and ABC surface. But at high concentrations, end-on formation, which is lateral to the surface, is favourable due to the cationic nitrogen in RhB at pH 4. These groups can be attached to the anionic functional groups of ABC surface forming strong ion–ion interactions.

3.2.4. Adsorption isotherms

Adsorption isotherms are generated at different temperatures from 300 to 330 K in order to optimize the parameters for practical applications. Based on the experimental data, the order of decrease in fitting isotherm models for RhB adsorption onto ABC were Langmuir > Temkin > Freundlich > D–R >> Sips models. Linearized graphs for these five isotherms are shown in Fig. 7.

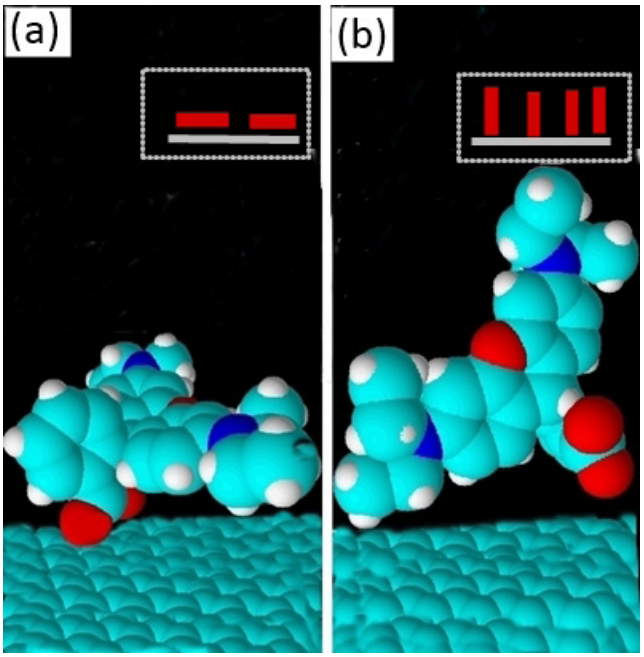

Fig. 6. Mechanism of adsorption of RhB onto ABC (a) flat orientation of RhB molecule at low RhB concentrations and (b) vertical orientation of RhB molecule at high RhB concentrations.

Langmuir isotherm considers mono-layer adsorption on solid surface, which has homogeneous sites [38]. Maximum adsorption capacity (q_{max}) at 300 K was 111.11 mg g^{-1} and increased with increasing temperature reaching a maximum value of 200 mg g^{-1} at 330 K. The observed Langmuir constant (K_L) values (Table 4), which are less than 1, show that ion exchange becomes the predominant mechanism, which confirms the endothermic nature of the adsorption process [17]. The K_L value is highest at 330 K, which indicates the best affinity of RhB onto ABC at this temperature. The maximum adsorption capacity obtained in this study was significantly higher than the values reported in the literature (Table 5).

Dimensionless adsorption intensity given in Eq. (12) is an indication of the feasibility of the reaction where $R_L > 1$, $R_L = 1$, $R_L < 1$ and $R_L = 0$ represent an unfavourable, linear, favourable and irreversible adsorption process, respectively [44]. Dimensionless adsorption intensities, R_L, calculated at different temperatures referring to the Eq. (12) are summarized in Table 6.

$$R_L = \frac{1}{1 + K_L C_0} \tag{12}$$

In this experiment, R_L is 0.057 for concentration of 50 mg L^{-1} at 300 K and decreases with increasing concentration and temperature. The relatively low R_L value indicates strong bond between the adsorbent and adsorbate, and the interactions become stronger with increasing concentration, and therefore, it indicates the possibility of end-on orientation at higher RhB concentrations.

On the other hand, according to the Temkin isotherm model, Gibbs energy value calculated using Eq. (13) at 300 K is –15.72 kJ mol^{-1}. The large negative value of Gibbs energy suggests that heat of adsorption of all molecules in the layer would decrease linearly with the surface coverage.

$$\Delta G^\circ = -RT\ln K_T \tag{13}$$

Moreover, Freundlich isotherm model and the value of parameter $1/n$ were used to understand surface heterogeneity and the favourability of the adsorption process. Adsorption process is unfavourable when $1/n > 1$ and favourable when $0 < 1/n < 1$, and homogeneous adsorption without interactions between the adsorbed species occurs when $1/n = 1$ [20]. This experiment gives $1/n$ as 0.12 (n = 8.31) at 300 K, which suggests a favourable adsorption on heterogeneous ABC surface.

D–R isotherm is based on the postulate that the mechanism of adsorption is a pore-filling activity rather than layer by layer filling and generally involving only van der Waals forces between the system and the adsorbent [45]. The coefficient of determination (R^2) value for D–R isotherm is low indicating low linearity, and hence, adsorption does not obey

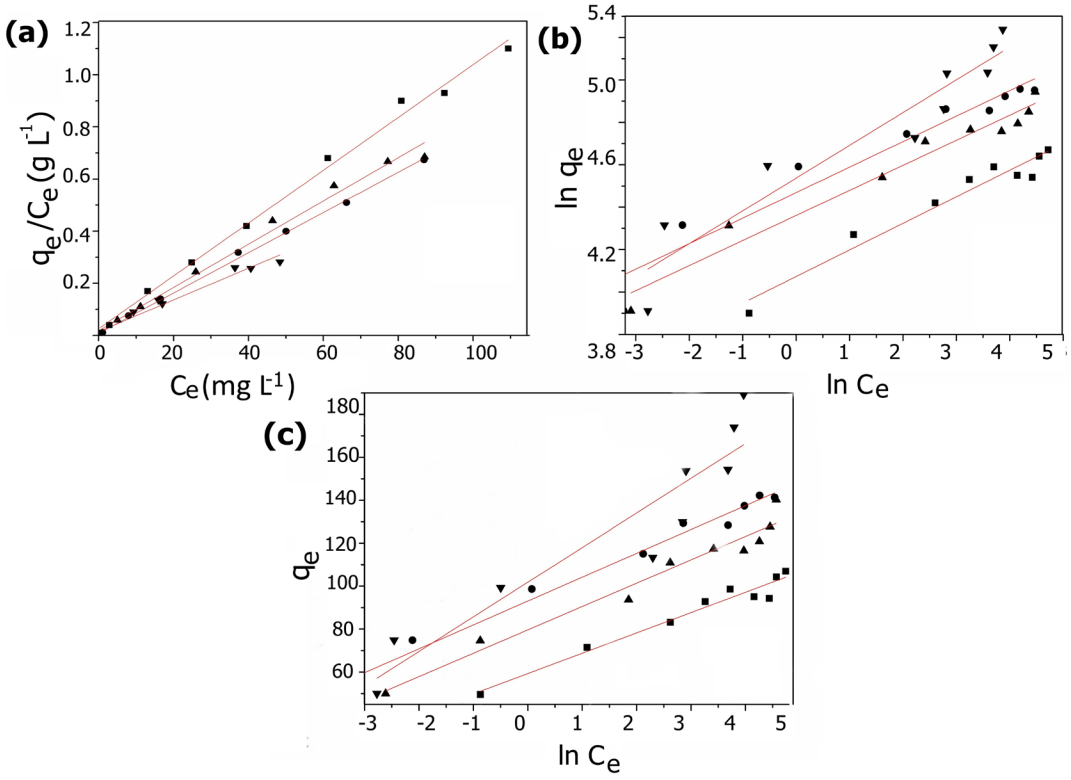

Fig. 7. Linearized (a) Langmuir, (b) Freundlich and (c) Temkin isotherms for RhB adsorption onto ABC at different temperatures (■300, ▲310, ●320 and ▼330 K).

Table 5
RhB adsorption capacity of different adsorbents

Precursor	Activation conditions	q_{max} at room temperature (mg g^{-1})	Reference
Pheonix sylvestris leaves	Sulphuric acid	51.6	[16]
Thespesia populnea bark	Sulphuric acid	60.8	[17]
Palm shell	CO_2 and then NaOH	62.6	[19]
Bamboo saw dust	Phosphoric acid	111.1	This work
Pyrolytic tire	Air	277.8	[18]
Rise husk	Phosphoric acid then KOH	478.5	[9]
Polygonum orientale Linn	Phosphoric acid	480	[39]
Other adsorbents			
Jack fruit seed		26.4	[40]
Kaolinite		46.1	[41]
Used tea leaves		53.2	[15]
Azolla pinnata		72.2	[42]
Casuarina equisetifolia needle		82.34	[43]
Peat		85.45	[14]

Table 6
Dimensionless adsorption intensity (R_L) at different temperatures

Co (mg L^{-1})	R_L			
	300 K	310 K	320 K	330 K
50	0.057	0.044	0.020	0.049
100	0.029	0.022	0.010	0.025
150	0.020	0.015	0.007	0.017

D–R isotherm. This confirms that van der Waals forces are not the predominant interaction type operating between RhB molecules and ABC.

Sips model is a combination of the Langmuir and Freundlich isotherm models. Sips model reduces to Freundlich isotherm at low RhB concentration and increases to Langmuir at high concentrations. The lowest R^2 value is for Sips model, which indicates that the adsorption does not obey Sips model.

3.2.5. Thermodynamic studies

The adsorption capacity of RhB onto ABC increases with increasing the temperature of the system (Fig. 8).

The negative values of $\Delta G°$ suggest that the adsorption process of RhB onto ABC is favourable and more favoured with the increase of temperature as the negative value of $\Delta G°$

Table 4
Adsorption isotherm parameters for the adsorption of RhB onto ABC

Isotherm model	Parameter	Temperature (K)			
		300	310	320	330
Langmuir	q_{max} (mg g^{-1})	111.11	142.86	142.86	200.00
	K_L (L mg^{-1})	0.333	0.438	1.000	0.385
	R^2	0.993	0.990	0.998	0.973
Freundlich	K_F (mg g^{-1})	46.81	31.50	34.88	93.50
	n	8.00	8.55	8.33	6.49
	R^2	0.954	0.961	0.937	0.908
Temkin	K_T (L mg^{-1})	546.55	3,168.79	4,114.67	528.83
	B (J mol^{-1})	9.39	10.31	11.22	16.33
	R^2	0.960	0.960	0.980	0.866
D–R	β (J mol^{-1})	7.00E–08	1.00E–08	1.00E–08	2.00E–08
	q_{max} (mg g^{-1})	92.94	114.55	50.70	145.18
	E (kJ mol^{-1})	2.673	7.071	7.071	5.000
	R^2	0.785	0.821	0.909	0.817
Sips	K_s	1.050	1.551	2.829	1.110
	1/n	0.500	0.404	0.610	0.394
	R^2	0.853	0.722	0.796	0.776

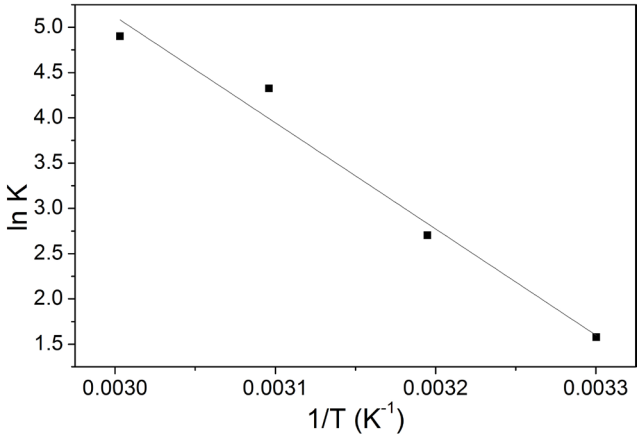

Fig. 8. Plot of ln K vs. 1/T for RhB adsorption onto ABC: [RhB] = 80 mg L^{-1}.

increases with the temperature. Referring to Table 7, ΔG° value of –20 kJ mol^{-1} was obtained in this adsorption.

Enthalpy and entropy values for the process were calculated referring to the Van 't Hoff equation (Eq. (10)).The positive value of ΔH° (95.63 kJ mol^{-1}) confirms the endothermic nature of the adsorption process while the ΔS° (331.98 kJ mol^{-1} K^{-1}) indicates the increased disorder, which confirms the structural change. As the solvent–RhB interactions are broken, the disorder of the system is increased, and then RhB–ABC interactions are generated via predominant ion–ion interactions.

3.3. Adsorption and desorption kinetic studies

Both adsorption and desorption kinetic studies were carried out proposing pseudo-first-order model, pseudo-second-order model and intraparticle diffusion model (Fig. 9)

Table 7
ΔG° values for RhB adsorption onto ABC

T (K)	ΔG° (kJ mol^{-1})
300	–19.52
310	–19.85
320	–20.17
330	–20.52

in order to understand the nature of the two processes. ABC was regenerated after the dye adsorption to make it more economical by recovering ABC and RhB. Ethanol is an effective solvent to remove RhB completely from ABC surface after repeated washings.

To interpret the pseudo-first-order kinetic model, log(q_e – q_t) was plotted against time by taking $q_{e,exp}$ as 62.315 mg g^{-1} for adsorption process and 2.540 mg g^{-1} for desorption process (Table 8). According to the results, the values of $q_{e,cal}$ (25.235 mg g^{-1} and 0.778 mg g^{-1} for adsorption and desorption, respectively) significantly deviate from experimental values. Also, the R^2 values (0.786 and 0.473 for adsorption and desorption, respectively) are significantly low, showing low linearity. This observation can be explained by referring to the study carried out by Ungarish and Aharoni [46], where he concludes that if adsorption is immeasurably slow, the adsorbed amount is less than the equilibrium amount. Consequently, the $q_{e,exp}$ is difficult to be measured as well as it is generally applicable only for initial 20–30 min [47]. Therefore, RhB adsorption onto ABC in aqueous media and RhB desorption from ABC in ethanol media do not follow pseudo-first-order kinetic model.

As illustrated in Fig. 9(b), both adsorption and desorption processes perfectly follow pseudo-second-order kinetic model. The $q_{e,cal}$ for adsorption (66.667 mg g^{-1}) is

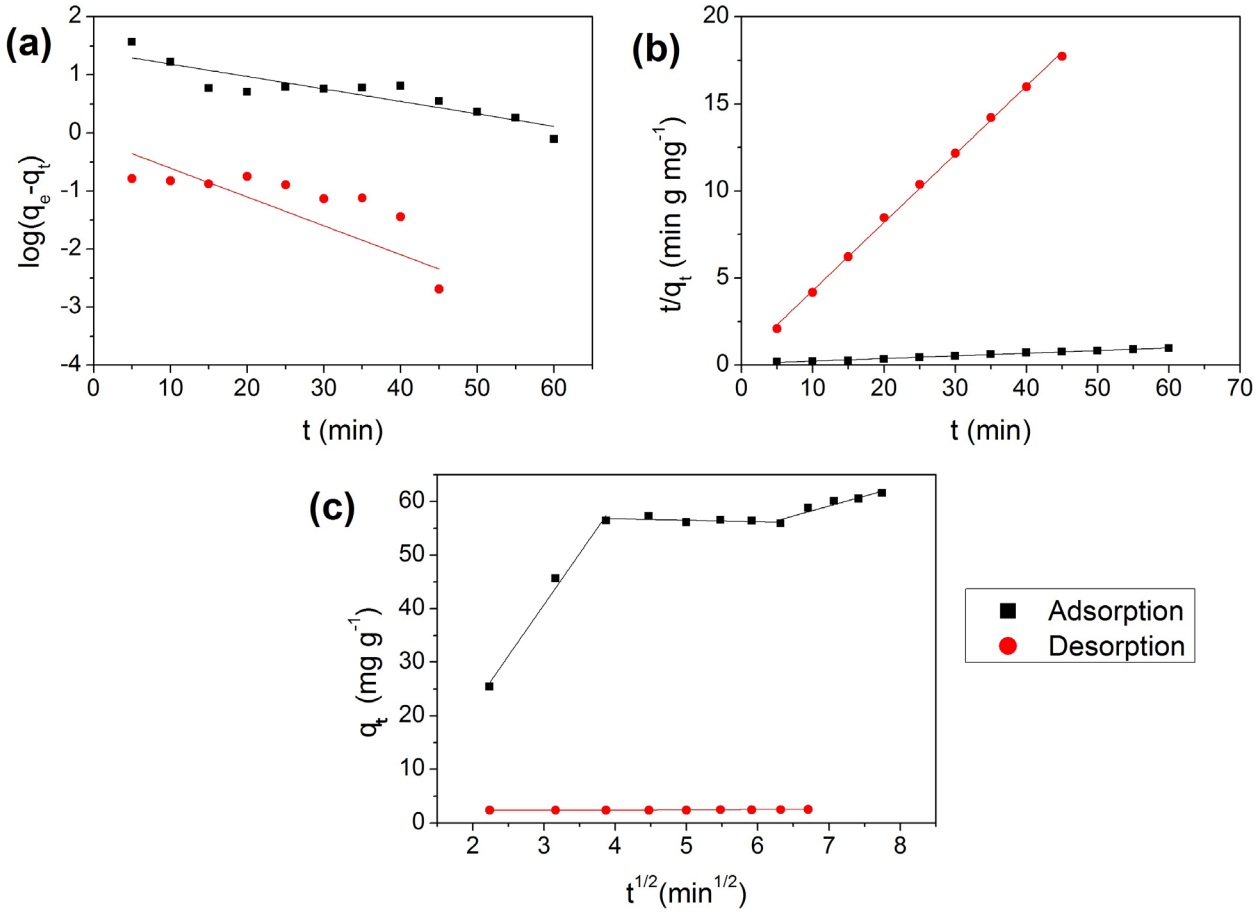

Fig. 9. The graphs of (a) pseudo-first-order, (b) pseudo-second-order and (c) intraparticle diffusion model at 300 K for adsorption and desorption processes.

Table 8
Kinetic model parameters for adsorption and desorption of RhB at 300 K

Kinetic model	Linear form of the equation	Kinetic parameters	
		Adsorption	Desorption
Pseudo-first-order model	$\log(q_e - q_t) = \log(q_e) - \frac{k_1}{2.303}t$	k_1 = 0.048 min^{-1} q_e = 25.235 mg g^{-1} R^2 = 0.786	k_1 = 0.114 min^{-1} q_e = 0.778 mg g^{-1} R^2 = 0.473
Pseudo-second-order model	$\frac{t}{q_t} = \frac{1}{k_2 q_e^2} + \frac{1}{q_e}t$	k_2 = 0.003 g min^{-1} mg^{-1} q_e = 66.667 g mg^{-1} R^2 = 0.992	k_2 = 0.448 g mg^{-1} min^{-1} q_e = 2.545 g mg^{-1} R^2 = 0.999
Intraparticle diffusion model	$q_t = k_{id}t^{1/2} + C$	k_{id} = 4.545 mg g^{-1} $min^{-1/2}$ C = 29.546 mg g^{-1} R^2 = 0.599	k_{id} = 0.035 mg g^{-1} $min^{-1/2}$ C = 2.270 mg g^{-1} R^2 = 0.696

agreed with experimental value, and $q_{e,exp}$ (62.315 mg g^{-1}) with highest R^2 value of 0.992. The $q_{e,cal}$ for desorption (2.545 mg g^{-1}) is agreed with experimental value, and $q_{e,exp}$ (2.540 mg g^{-1}) with highest R^2 value of 0.999. This indicates that adsorption process of RhB on ABC surface perfectly follows pseudo-second-order kinetics and rate-limiting step may be the desorption of chemisorbed dye molecules [48].

If intraparticle diffusion completely governs the adsorption and desorption processes, the plot should be linear, and if the rate-limiting step is only intraparticle diffusion, the plot should pass through the origin [49]. When considering the results given above, the plots in Fig. 9(c) are not linear during the complete range of time (R^2 is 0.599 for adsorption). However, three distinguishable main linear sections can be identified in adsorption curve. Therefore, it can be concluded

that intraparticle diffusion is not the only rate-limiting step in the adsorption process of RhB onto ABC surface. This can be caused by the external mass transfer followed by intraparticle diffusion. The three possible major steps are external mass transfer from the bulk solution, intraparticle diffusion and adsorption of dye molecules [50]. As the lines do not pass through the origin, it can be concluded that the above three events do not occur, simultaneously.

4. Conclusion

In this study, bamboo carbon originated from *Bambusa vulgaris* stems were chemically activated using phosphoric acid activation method, and the resulting ABC was effectively used for the removal of RhB from aqueous solutions.

ABC consists of active functional groups such as alcohols, phenols, carboxylic acids, alkynes, alkenes, esters, ethers, phosphate ethers and phosphate esters, and their presence was confirmed by the FTIR technique. Boehm titration further provided evidence for the existence of both basic and acidic functional groups. PXRD characterization suggested a graphitic layered structure, and the resulting ABC demonstrated an amorphous nature. Phosphoric acid activated ABC has a highly porous structure with different size pores ranging from submicro- to nano-scale, thus leading to a high surface area. Iodine value test corroborated the evidences provided by TEM analysis.

For adsorption of RhB, the estimated contact time of 105 min followed by 1 h settling time and pH of 6 and 8 were found to be the best condition for maximum adsorption. The best fit adsorption isotherm was Langmuir model (L4 type), suggesting the adsorption mechanism as the RhB molecules initially adsorb flat onto ABC surface followed by end-on orientation with increasing concentration. The maximum adsorption capacity was 111.11 mg g^{-1} at 300 K and increased with increasing temperature. The Freundlich and Temkin models were also fitted to the adsorption process. Thermodynamic results, negative $\Delta G°$ values, show the feasibility of the adsorption process while positive $\Delta H°$ and positive $\Delta S°$ values show the endothermic nature and increasing entropy, respectively. The best fitted kinetic model for both adsorption and desorption was pseudo-second-order model suggesting the rate-limiting step could be chemisorption.

Acknowledgement

Authors acknowledge CSIR-Central Salt & Marine Chemicals Research Institute, Gujarat, India, for providing imaging facilities.

References

[1] R. Bushra, M. Naushad, R. Adnan, Z.A. ALOthman, M. Rafatullah, Polyaniline supported nanocomposite cation exchanger: synthesis, characterization and applications for the efficient removal of Pb^{2+} ion from aqueous medium, J. Ind. Eng. Chem., 21 (2015) 1112–1118.

[2] T.A. Khan, E.A. Khan, Removal of basic dyes from aqueous solution by adsorption onto binary iron-manganese oxide coated kaolinite: non-linear isotherm and kinetics modeling, Appl. Clay Sci., 107 (2015) 70–77.

[3] L.B.L. Lim, N. Priyantha, T. Zehra, C.W. Then, C.M. Chan, Adsorption of crystal violet dye from aqueous solution onto chemically treated *Artocarpus odoratissimus* skin: equilibrium, thermodynamics, and kinetics studies, Desal. Wat. Treat., 57 (2016) 10246–10260.

[4] M. Naushad, T. Ahamad, G. Sharma, A.H. Al-Muhtaseb, A.B. Albadarin, M.M. Alam, Z.A. ALOthman, S.M. Alshehri, A.A. Ghfar, Synthesis and characterization of a new starch/ SnO_2 nanocomposite for efficient adsorption of toxic Hg^{2+} metal ion, Chem. Eng. J., 300 (2016) 306–316.

[5] O. Sulaiman, N.S. Ghani, M. Rafatullah, R. Hashim, Removal of zinc (II) ions from aqueous solutions using surfactant modified bamboo sawdust, Sep. Sci. Technol., 46 (2011) 2275–2282.

[6] T.A. Khan, S. Sharma, E.A. Khan, A.A. Mukhlif, Removal of congo red and basic violet 1 by chir pine (*Pinus roxburghii*) sawdust, a saw mill waste: batch and column studies, Toxicol. Environ. Chem., 96 (2014) 555–568.

[7] M. Naushad, M.R. Khan, Z.A. ALOthman, I. AlSohaimi, F. Rodriguez-Reinoso, T.M. Turki, R. Ali, Removal of BrO_3^- from drinking water samples using newly developed agricultural waste-based activated carbon and its determination by ultra-performance liquid chromatography-mass spectrometry, Environ. Sci. Pollut. Res., 22 (2015) 15853–15865.

[8] K.Y. Foo, B.H. Hameed, Mesoporous activated carbon from wood sawdust by K_2CO_3 activation using microwave heating, Bioresour. Technol., 111 (2012) 425–432.

[9] L. Ding, B. Zou, W. Gao, Q. Liu, Z. Wang, Y. Guo, X. Wang, Y. Liu, Adsorption of Rhodamine-B from aqueous solution using treated rice husk-based activated carbon, Colloids Surf., A, 446 (2014) 1–7.

[10] Z.A. ALOthman, M. Naushad, R. Ali, Kinetic, equilibrium isotherm and thermodynamic studies of Cr(VI) adsorption onto low-cost adsorbent developed from peanut shell activated with phosphoric acid, Environ. Sci. Pollut. Res., 20 (2013) 3351–3365.

[11] E. Hettiarachchi, R. Perera, A.D.L.C. Perera, N. Kottegoda, Activated coconut coir for removal of sodium and magnesium ions from saline water, Desal. Wat. Treat., 57 (2016) 22341–22352.

[12] D. Pathania, G. Sharma, A. Kumar, M. Naushad, S. Kalia, A. Sharma, Z.A. ALOthman, Combined sorptional–photocatalytic remediation of dyes by polyaniline Zr(IV) selenotungstophosphate nanocomposite, Toxicol. Environ. Chem., 97 (2015) 526–537.

[13] A. Kumar, G. Sharma, M. Naushad, P. Singh, S. Kalia, Polyacrylamide/$Ni_{0.02}Zn_{0.98}O$ nanocomposite with high solar light photocatalytic activity and efficient adsorption capacity for toxic dye removal, Ind. Eng. Chem. Res., 53 (2014) 15549–15560.

[14] H.I. Chieng, L.B.L. Lim, N. Priyantha, Sorption characteristics of peat from Brunei Darussalam for the removal of rhodamine B dye from aqueous solution: adsorption isotherms, thermodynamics, kinetics and regeneration studies, Desal. Wat. Treat., 55 (2015) 664–677.

[15] M.A. Hossain, M.S. Alam, Adsorption kinetics of Rhodamine-B on used black tea leaves, Iran. J. Environ. Health Sci. Eng., 9 (2012) 1–7.

[16] S. Arivoli, M. Henkuzhali, Kinetic, mechanistic, thermodynamic and equilibrium studies on the adsorption of Rhodamine B by acid activated low cost carbon, J. Chem., 5 (2008) 187–200.

[17] M. Hema, S. Arivoli, Rhodamine B adsorption by activated carbon: kinetic and equilibrium studies, Indian J. Chem. Technol., 16 (2009) 38–45.

[18] L. Li, S. Liu, T. Zhu, Application of activated carbon derived from scrap tires for adsorption of Rhodamine B, J. Environ. Sci., 22 (2010) 1273–1280.

[19] M. Mohammadi, A.J. Hassani, A.R. Mohamed, G.D. Najafpour, Removal of Rhodamine B from aqueous solution using palm shell-based activated carbon: adsorption and kinetic studies, J. Chem. Eng. Data., 55 (2010) 5777–5785.

[20] F.Y. Wang, H. Wang, J.W. Ma, Adsorption of cadmium (II) ions from aqueous solution by a new low-cost adsorbent—Bamboo charcoal, J. Hazard. Mater., 177 (2010), 300–306.

[21] Q.S. Liu, T. Zheng, N. Li, N.P. Wang, G. Abulikemu, Modification of bamboo-based activated carbon using microwave radiation and its effects on the adsorption of methylene blue, Appl. Surf. Sci., 256 (2010) 3309–3315.

[22] B.H. Hameed, A.T. Din, A.L. Ahmad, Adsorption of methylene blue onto bamboo-based activated carbon: kinetics and equilibrium studies, J. Hazard. Mater., 141 (2007) 819–825.
[23] F.C. Yang, K.H. Wu, W.P. Lin, M.K. Hu, T.S. Sheu, D.N. Horng, Preparation and antibacterial effect of bamboo charcoal/Ag on *Staphylococcus aureus* and *Pseudomonas aeruginosa*, J. Chin. Chem. Soc., 56 (2009) 327–334.
[24] T.M. Disanayake, N. Kottegoda, C. Perera, Evaluation of ion adsorption capacities of Murunkan clay and coir as cost effective materials for desalination of water, Int. J. Earth Sci. Eng., 6 (2013) 788–790.
[25] E. Hettiarachchi, N. Kottegoda, A.D.L.C. Perera, Activated coir for removal of water hardness, Desal. Wat. Treat., (2017) 1–8. doi: 10.5004/dwt.2017.0339.
[26] A. Paragodaarachchi, A.D.L.C. Perera, N. Kottegoda, Flouride Adsorption on Activated Coconut Coir, Proc. Research and Development Study Symposium, World Water Day, Colombo, Sri Lanka, 2016.
[27] Q.S. Liu, T. Zheng, P. Wang, L. Guo, Preparation and characterization of activated carbon from bamboo by microwave-induced phosphoric acid activation, Ind. Crops Prod., 31 (2010) 233–238.
[28] H. Boehm, Some aspects of the surface chemistry of carbon blacks and other carbons, Carbon, 32 (1994) 759–769.
[29] L.S. Chan, W.H. Cheung, G. McKay, Adsorption of acid dyes by bamboo derived activated carbon, Desalination, 218 (2008) 304–312.
[30] E. Cristiano, Y.J. Hu, M. Siegfried, D. Kaplan, H. Nitsche, A comparison of point of zero charge measurement methodology, Clays Clay Miner., 59 (2011) 107–115.
[31] H. Boehm, Surface oxides on carbon and their analysis: a critical assessment, Carbon, 40 (2002) 145–149.
[32] A. Puziy, O. Poddubnaya, A. Martınez-Alonso, F. Suárez-Garcıa, J. Tascón, Synthetic carbons activated with phosphoric acid: I. Surface chemistry and ion binding properties, Carbon, 40 (2002) 1493–1505.
[33] Y. Wang, X. Wang, M. Liu, X. Wang, Z. Wu, L. Yang, S. Xia, J. Zhao, Cr(VI) removal from water using cobalt-coated bamboo charcoal prepared with microwave heating, Ind. Crops Prod., 39 (2012) 81–88.
[34] C.H. Giles, T. MacEwan, S. Nakhwa, D. Smith, 786. Studies in adsorption. Part XI. A system of classification of solution adsorption isotherms, and its use in diagnosis of adsorption mechanisms and in measurement of specific surface areas of solids, J. Chem. Soc. (1960) 3973–3993. doi:10.1039/JR9600003973.
[35] E. Lorenc-Grabowska, P. Rutkowski, High basicity adsorbents from solid residue of cellulose and synthetic polymer copyrolysis for phenol removal: kinetics and mechanism, Appl. Surf. Sci., 316 (2014) 435–442.
[36] R. Otero, D. Esquivel, M.A. Ulibarri, F.J. Romero-Salguero, P. Van Der Voort, J.M. Fernández, Mesoporous phenolic resin and mesoporous carbon for the removal of S-Metolachlor and Bentazon herbicides, Chem. Eng. J., 251 (2014) 92–101.
[37] J.M.L. Martínez, M.F.L. Denis, L.L. Piehl, E.R. de Celis, G.Y. Buldain, V.C. Dall' Orto, Studies on the activation of hydrogen peroxide for color removal in the presence of a new Cu(II)-polyampholyte heterogeneous catalyst, Appl. Catal., B, 82 (2008) 273–283.
[38] I. Langmuir, The adsorption of gases on plane surfaces of glass, mica and platinum, J. Am. Chem. Soc., 40 (1918) 1361–1403.
[39] L. Wang, J. Zhang, R. Zhao, C. Li, Y. Li, C. Zhang, Adsorption of basic dyes on activated carbon prepared from *Polygonum orientale* Linn: equilibrium, kinetic and thermodynamic studies, Desalination, 254 (2010) 68–74.
[40] M.R.R. Kooh, M.K. Dahri, L.B.L. Lim, Jackfruit seed as a sustainable adsorbent for the removal of Rhodamine B dye, J. Environ. Biotechnol. Res., 4 (2016) 7–16.
[41] T.A. Khan, S. Dahiya, I. Ali, Use of kaolinite as adsorbent: equilibrium, dynamics and thermodynamic studies on the adsorption of Rhodamine B from aqueous solution, Appl. Clay Sci., 69 (2012) 58–66.
[42] M.R.R. Kooh, L.B.L. Lim, L.H. Lim, M.K. Dahri, Separation of toxic rhodamine B from aqueous solution using an efficient low-cost material, Azolla pinnata, by adsorption method, Environ. Monit. Assess., 188 (2016) 1–15.
[43] M.R.R. Kooh, M.K. Dahri, L.B.L. Lim, The removal of rhodamine B dye from aqueous solution using *Casuarina equisetifolia* needles as adsorbent, Cogent Environ. Sci., 2 (2016) 1140553. doi: 10.1080/23311843.2016.1140553.
[44] K. Foo, B. Hameed, Insights into the modeling of adsorption isotherm systems, Chem. Eng. J., 156 (2010) 2–10.
[45] N.D. Hutson, R.T. Yang, Theoretical basis for the Dubinin-Radushkevitch (D–R) adsorption isotherm equation, Adsorption, 3 (1997) 189–195.
[46] M. Ungarish, C. Aharoni, Kinetics of chemisorption. Deducing kinetic laws from experimental data, J. Chem. Soc., Faraday Trans. 1, 77 (1981) 975–985.
[47] S. Azizian, Kinetic models of sorption: a theoretical analysis, J. Colloid Interface Sci., 276 (2004) 47–52.
[48] H.M. Gad, A.A. El-Sayed, Activated carbon from agricultural by-products for the removal of Rhodamine-B from aqueous solution, J. Hazard. Mater., 168 (2009) 1070–1081.
[49] Y. Ho, J. Ng, G. McKay, Kinetics of pollutant sorption by biosorbents: review, Sep. Purif. Methods, 29 (2000) 189–232.
[50] Y. Ho, G. McKay, A comparison of chemisorption kinetic models applied to pollutant removal on various sorbents, Process Saf. Environ. Prot., 76 (1998) 332–340.